J|A|C|S
ARTICLES
Published on Web 02/28/2007

Molecular Wiring of Insulators: Charging and Discharging Electrode Materials for High-Energy Lithium-Ion Batteries by Molecular Charge Transport Layers

Qing Wang,[†] Nick Evans,[†] Shaik M. Zakeeruddin,[†] Ivan Exnar,[‡] and Michael Grätzel*,[†]

Contribution from the Laboratory for Photonics and Interfaces, Ecole Polytechnique Fédérale de Lausanne, CH-1015 Lausanne, Switzerland, and HPL SA, CH-1015 Lausanne, Switzerland

Received August 29, 2006; E-mail: michael.graetzel@epfl.ch

Abstract: Self-assembled monolayers (SAMs) of redox-active molecules on mesoscopic substrates exhibit two-dimensional conductivity if their surface coverage exceeds the percolation threshold. Here, we show for the first time that such molecular charge transport layers can be employed to electrochemically address insulating battery materials. The widely used olivine-structured $LiFePO_4$ was derivatized with a monolayer of 4-[bis(4-methoxyphenyl)amino]benzylphosphonic acid (BMABP) in this study. Fast cross-surface hole percolation was coupled to interfacial charge injection, affording charging and discharging of the cathode material. These findings offer the prospect to greatly reduce the amount of conductive carbon additives necessary to electrochemically address present metal phosphate cathode materials, opening up the possibility for a much improved energy storage density. When compared at equal loading, the rate capability is also enhanced with respect to conventional carbon-based conductive additives.

Introduction

Lithium-ion batteries are the state-of-the-art power sources for portable electronic devices. Lithium insertion materials are preferred over Li-metal, at the expense of energy storage capacity, for reasons of better cyclability and safety.[1] A notorious problem arises from the poor electronic conductivity of the currently used lithium insertion materials. To exploit its full capacity, large quantities of conductive additives, such as carbon black or graphite, have to be used to improve the electronic conductivity. Sometimes the conductive additives occupy practically half of the volume of the active materials to form a continuous conduction network, greatly decreasing the energy density of the cell. This situation is even more severe for the new generation cathodic materials, olivine-type $LiMPO_4$ (M = Fe, Co, Ni, Mn), because of their extremely low electronic conductivity (σ, $\sim 10^{-9}$ S cm^{-1}).[2] For this reason, great endeavors are being made to increase the conductivity of the cathode materials, for example, carbon coating[2b,3] and supervalent cation doping.[2c] However, so far the success of these strategies has been very limited, a large amount of carbon still being needed to afford reasonable battery performance.

Molecular wiring of battery materials is based on our recent discovery of cross-surface electron and hole transfer in self-assembled molecular charge transport layers on mesoscopic oxide films.[4] Charge propagation within the surface-confined monolayer proceeds by thermally activated electron hopping between adjacent molecules. At the same time, counterions in the electrolyte diffuse to compensate the charge of the oxidized molecules. A macroscopic conduction pathway is formed once the coverage of the oxide nanoparticles by the electro-active species exceeds 50%.[4−6] Here, we show for the first time that such molecular charge transport layers can be employed to electrochemically address insulating battery materials, the material of choice being triphyllite, that is, lithium iron phosphate ($LiFePO_4$). Strikingly, our findings demonstrate that a single molecular layer of a suitable redox-active molecule alone can provide the desired electronic charge transport while still permitting lithium ion exchange to occur rapidly across

[†] Ecole Polytechnique Fédérale de Lausanne.
[‡] HPL SA.

(1) (a) Tarascon, J.-M.; Armand, M. *Nature* **2001**, *414*, 359. (b) Whittingham, M. S. *Chem. Rev.* **2004**, *104*, 4271.
(2) (a) Padhi, A. K.; Nanjundaswamy, K. S.; Goodenough, J. B. *J. Electrochem. Soc.* **1997**, *144*, 1188. (b) Tarascon, J.-M.; et al. *Dalton Trans.* **2004**, 2988. (c) Chung, S.-Y.; Bloking, J. T.; Chiang, Y.-M. *Nat. Mater.* **2002**, *1*, 123. (d) Herle, P. S.; Ellis, B.; Coombs, N.; Nazar, L. F. *Nat. Mater.* **2004**, *3*, 147. (e) Delacourt, C.; Laffont, L.; Bouchet, R.; Wurm, C.; Leriche, J.-B.; Morcrette, M.; Tarascon, J.-M.; Masquelier, C. *J. Electrochem. Soc.* **2005**, *152*, A913.
(3) (a) Huang, H.; Yin, S. C.; Nazar, L. F. *Electrochem. Solid-State Lett.* **2001**, *4*, A170. (b) Chen, Z. H.; Dahn, J. R. *J. Electrochem. Soc.* **2002**, *149*, A1184. (c) Doeff, M. M.; Hu, Y. Q.; McLarnon, F.; Kostecki, R. *Electrochem. Solid-State Lett.* **2003**, *6*, A207. (d) Yang, J. S.; Xu, J. J. *Electrochem. Solid-State Lett.* **2004**, *7*, A515. (e) Mi, C. H.; Cao, G. S.; Zhao, X. B. *Mater. Lett.* **2005**, *59*, 127. (f) Dominko, R.; Bele, M.; Gaberscek, M.; Remskar, M.; Hanzel, D.; Pejovnik, S.; Jamnik, J. *J. Electrochem. Soc.* **2005**, *152*, A607. (g) Mi, C. H.; Zhao, X. B.; Cao, G. S.; Tu, J. P. *J. Electrochem. Soc.* **2005**, *152*, A483. (h) Belharouak, I.; Johnson, C.; Amine, K. *Electrochem. Commun.* **2005**, *7*, 983. (i) Gabrisch, H.; Wilcox, J. D.; Doeff, M. M. *Electrochem. Solid-State Lett.* **2006**, *9*, A360.
(4) (a) Bonhôte, P.; Gogniat, E.; Tingry, S.; Barbé, C.; Vlachopoulos, N.; Lenzmann, F.; Comte, P.; Grätzel, M. *J. Phys. Chem. B* **1998**, *102*, 1498. (b) Wang, Q.; Zakeeruddin, S. M.; Cremer, J.; Bäuerle, P.; Humphry-Baker, R.; Grätzel, M. *J. Am. Chem. Soc.* **2005**, *127*, 5706. (c) Wang, Q.; Zakeeruddin, S. M.; Nazeeruddin, Md. K.; Humphry-Baker, R.; Grätzel, M. *J. Am. Chem. Soc.* **2006**, *128*, 4446.
(5) Trammell, S. A.; Meyer, T. J. *J. Phys. Chem. B* **1999**, *103*, 104.
(6) Sahimi, M. *Application of Percolation Theory*; Taylor & Francis: London, 1994; pp 1−22.

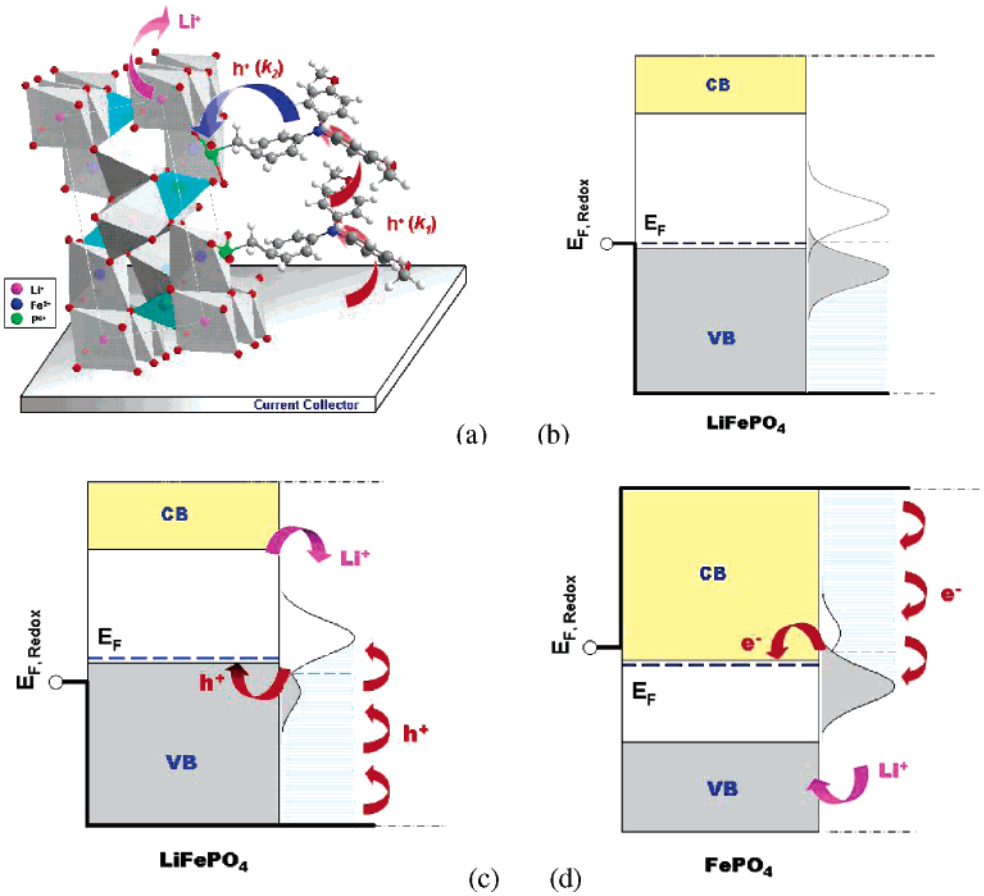

Figure 1. Band and density of states (DOS) diagrams showing the working principle of charging and discharging of an insulating battery material by a surface-confined molecular charge transport layer. The shaded and unshaded Gaussian functions represent the occupied and unoccupied electronic states of the redox relay, their intersection defining the Fermi level of the molecular hole transporter. (a) Structure of $LiFePO_4$ and the triarylamine (BMABP) substituted by a benzylic phosphonate anchoring group acting as molecular charge transport material. (b) Band diagram and density of electronic states (DOS) curves of the integrated electrode system at equilibrium. (c) Charging the cathode by hole propagation through the molecular monolayer; hole injection from $BMABP^+$ into $LiFePO_4$ and Li^+ release from $LiFePO_4$. (d) Discharging the electrode by reversing these three processes.

the solid/electrolyte interface. As compared to the total electrode size, the space occupied by the molecular charge transport layer is negligibly small, which greatly reduces the volume of conductive additive, opening up the possibility to increase substantially the energy storage density and rate capability at equal amounts of loading of conductive additives.

Experimental Section

Synthesis. The synthesis and characterization of 4-[bis(4-methoxyphenyl)amino]benzylphosphonic acid (BMABP) will be published elsewhere.

Electrode Preparation and Characterization. $LiFePO_4$ powder was synthesized by a solid-state reaction and ball-milled to reduce the particle size. The BET surface area of the powder is ~5 m^2/g with an average particle size of ~400 nm. The electrode was prepared by mixing the $LiFePO_4$ powder with 5 wt % PVDF and stirring with *N*-methyl-2-pyrrolidone (NMP). The resulting homogeneous slurry was then doctor-bladed onto F-doped conducting glass (FTO). After being dried in an oven at 100 °C overnight, the films were cut into smaller pieces of 0.8 cm^2. The typical thickness of the film was 5−7 μm. The preparation of mesoscopic Al_2O_3 film has been described in ref 4a and the BET area being 235 m^2/g.

BMABP solution was prepared in a glovebox by dissolving the compound in acetonitrile with a concentration of 1 mM. The $LiFePO_4$ electrodes were then dipped into the above solution for 3 h. The derivatized electrodes were rinsed in acetonitrile to remove any weakly adsorbed molecules. Subsequently, the electrode sheets were treated on a hot plate at around 100 °C for 2 h. The whole process was carried out in an argon-filled glovebox. The derivatization of Al_2O_3 films followed a similar procedure.

The surface coverage of $LiFePO_4$ by BMABP was determined by UV/vis spectroscopy using a Cary 5 spectrophotometer. The uptake of BMABP by $LiFePO_4$ was derived from the change in the absorbance of the solution. The area occupied by a BMABP molecule at full monolayer coverage and the adsorption constant were determined by fitting the data to a Langmuir isotherm.

ATR-FTIR analysis employed a FTS700 FTIR spectrometer (Digilab, U.S.). Samples were measured under a mechanical force pressing the surface against the diamond window. Spectra were derived from 64 scans at a resolution of 4 cm^{-1}. Prior to measuring the spectra, the derivatized films were rinsed in acetonitrile to wash out any weakly adsorbed molecules and dried.

Voltammetric and impedance measurements employed a PC-controlled AutoLab PSTA30 electrochemical workstation (Eco Chimie) with counter and reference electrodes of lithium foil. The electrolyte was an ethylene carbonate (EC)/diethylcarbonate (DEC) mixture (1:1 in volume) with 0.5 M, 1 M, and saturated $LiPF_6$. The galvanic measurements were performed with a PC-controlled VoltaLab PGZ301 (Radiometer Analytical SA).

Results and Discussion

Figure 1 outlines the principle of addressing electrochemically the cathode material via cross-surface conduction through the electro-active molecular layer. To achieve fast charge percola-

tion, the electron exchange reaction between adjacent anchored molecules should be characterized by strong electronic coupling and a low reorganization energy.[4c,7] Also, interfacial charge transfer between the anchored molecule and the substrate material should be fast and reversible. Finally, to be able to withdraw electrons from the olivine during the charging step and return them during the discharging step, its redox potential should closely match the Fermi level of the battery material. The latter is given by the Nernst equation:

$$E = E^{\Theta} + \frac{RT}{F} \ln \frac{a_{OX}}{a_{RE}} \quad (1)$$

which in view of the electrode reaction

$$LiMPO_4 \rightleftharpoons Li^+ + MPO_4 + e^- \quad (2)$$

reduces to:

$$E = E^{\Theta} + \frac{RT}{F} \ln a_{Li^+} \quad (3)$$

Thus, the Nernst potential of olivine is fixed by the Li^+ activity in the electrolyte. For $LiFePO_4$, it becomes equal to the standard potential of ~3.45 V (vs Li^+/Li) when $a_{Li^+} = 1$. Changing the Li^+ concentration enables a precise adjustment of the olivine potential to equal that of the redox relay. For a saturated (>1.5 M) solution of $LiPF_6$ in an EC+DEC (1:1) solvent mixture, the Fermi level of $LiFePO_4$ matches closely the redox potential of the BMABP/$BMABP^+$ couple. On the other hand, in 0.5 M $LiPF_6$ electrolyte, the $LiFePO_4$ Fermi level is reduced by about 30 mV due to the lowering of the Li^+ activity.

We have identified several molecular relays from the phenothiazine and triarylamine families that satisfy the aforementioned requirements. The following study focuses on the molecular hole conductor 4-[bis(4-methoxyphenyl)amino]-benzylphosphonic acid (BMABP). The standard redox potential of the BMABP/$BMABP^+$ couple, $E^\circ = 3.5$ V (vs Li^+/Li), closely matches that of the triphyllite. Figure 1a shows the structure of BMABP anchored to the surface of $LiFePO_4$ via the phosphonate side group.[8] UV/vis spectroscopy and Langmuir isotherm (Figure S1) measurements indicate that the molecule readily forms a monolayer on the surface of $LiFePO_4$ after the film is immersed in an acetonitrile solution of BMABP. At full coverage, one BMABP molecule occupies an area of ~0.4 nm^2 in agreement with expectations. Figure S2 compares the FTIR spectra of BMABP adsorbed on $LiFePO_4$ and mesoscopic Al_2O_3 films. Vibrations from C=C ring stretching at 1504 cm^{-1} and C−N stretching at 1239 cm^{-1} are clearly seen in the spectra for both samples. The signal from the BMABP-derivatized $LiFePO_4$ film is around 40 times weaker than that of the mesoscopic Al_2O_3 film, consistent with the difference in their BET surface areas.

At equilibrium, the electrochemical potential of the molecular hole transporter is equal to that of $LiFePO_4$, Figure 1b. The latter being a p-type semiconductor of 3.7 eV band gap,[9] the Fermi level is drawn close to its valence band edge. During charging of the battery, a positive polarization is applied to the electrode, resulting in the oxidation of BMABP. This moves its redox potential above the Fermi level of the solid, thereby providing the driving force for hole injection from the $BMABP^+$ into the valence band of $LiFePO_4$. At the same time, Li^+ is ejected, Figure 1c. Conversely, during discharging the electron transfer from the current collector into the molecular charge transport film reduces its potential below the Fermi level of $LiFePO_4$. As a consequence, electrons are injected from an occupied orbital of the molecule into the conduction band of the n-type $FePO_4$, and Li^+ is inserted concomitantly, Figure 1d.

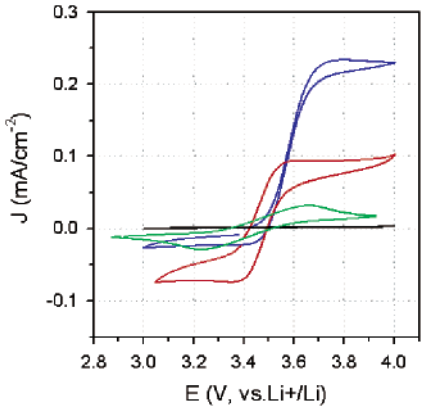

Figure 2. Cyclic voltammograms (CV) of BMABP-derivatized $LiFePO_4$ (red, blue) and mesoscopic Al_2O_3 (green) electrodes. The black line shows the curve of a bare $LiFePO_4$ electrode. The scan rate is 0.1 V/s. The current of BMABP-derivatized mesoscopic Al_2O_3 has been normalized according to its surface area. The electrolyte was a saturated solution of $LiPF_6$ in a 1:1 (w/w) mixture of ethylene carbonate (EC) and diethylcarbonate (DEC) except for the blue curve, where 0.5 M $LiPF_6$ was used.

Electrochemical experiments illustrating the charging and discharging of $LiFePO_4$ by cross-surface hole transfer are shown in Figure 2. The black line was obtained with the bare $LiFePO_4$ electrode using $LiPF_6$ (sat.)/EC+DEC (1:1) as electrolyte. The absence of any current response during the CV measurement confirms that $LiFePO_4$ is electrochemically inactive due to its insulating character. The current remains very low even after mixing the triphyllite particles with 1% carbon to enhance their conductivity. Strikingly, upon derivatization of the $LiFePO_4$ electrode with the molecular hole transporter BMABP, high oxidation and reduction currents are observed that can be attributed to charging and discharging of $LiFePO_4$ by cross-surface charge percolation. The features of the cyclic voltammogram are typical of catalytic waves, sustained oxidation and reduction currents being observed in the two plateau regions. The anodic current rises sharply upon polarizing the electrode above 3.5 V due to the oxidation of BMABP to $BMABP^+$. The appearance of a current plateau shows that BMABP is regenerated by hole injection into the $LiFePO_4$ and simultaneous release of Li^+ as shown in Figure 1c.

$$BMABP^+ + LiFePO_4 \rightleftharpoons BMABP + FePO_4 + Li^+ \quad (4)$$

The fact that the anodic current is sustained on a steady level confirms that the insulating $LiFePO_4$ can be charged by this interfacial hole injection following cross-surface charge transfer within the BMABP molecular layer. The diffusion coefficient for hole percolation was calculated to be ca. 10^{-8} cm^2/s from

(7) Marcus, R. A.; Sutin, N. *Biochim. Biophys. Acta* **1985**, *811*, 265.
(8) Gawalt, E. S.; Avaltron, M. J.; Koch, N.; Schwartz, J. *Langmuir* **2001**, *17*, 5736.
(9) Zhou, F.; Kang, K.; Maxisch, T.; Ceder, G.; Morgan, D. *Solid State Commun.* **2004**, *132*, 181.

the dependence of the forward current step on the scan rates (see Figure S3).[4c,10]

The reverse of reaction 4, corresponding to the discharge of the battery material, takes place when the electrode potential is brought below 3.5 V. Electron injection into $LiFePO_4$ associated with lithium uptake manifests itself by a cathodic current rising sharply with decreasing potential to again attain a plateau, whose value is similar to that of the anodic current. The blue curve in Figure 2 was obtained with a 0.5 M $LiPF_6$/EC+DEC (1:1) electrolyte. Here, the height of the anodic current plateau is greatly enhanced at the expense of the cathodic current signal. This behavior is expected because reducing the Li^+ concentration lowers the Fermi level of the $LiFePO_4$, increasing the driving force for the oxidation of $LiFePO_4$ by $BMABP^+$, while that of the reduction of $FePO_4$ by BMABP is decreased. This facilitates hole injection from $BMABP^+$ while the reverse process is impaired.

Importantly, when BMABP is anchored onto an electrochemically inert mesoscopic Al_2O_3 support, the CV (shown by the green curve in Figure 2) exhibits current peaks typical for a system where oxidation and reduction of the molecular relay are only coupled to diffusion. There is no evidence for interfacial charge exchange between the molecular charge-transfer layer and the Al_2O_3 solid in agreement with expectations. The normalized current density is more than 3 times lower than that of the BMABP-derivatized $LiFePO_4$, taking into account the 46 times greater BET surface of the mesoscopic Al_2O_3 electrode. A similar experiment employed a film of $LiMnPO_4$ particles,[11] which had a surface area comparable to that of $LiFePO_4$ but is redox-inert in the investigated potential range. The results corroborate our findings obtained with the Al_2O_3 support (see Figure S3).

The kinetic processes of the molecularly wired electrode are clearly depicted by electrochemical impedance spectroscopic measurements. The equivalent circuit shown in the inset of Figure 3 includes two transmission lines describing semi-infinite length diffusion of charge carriers through the molecular monolayer and diffusion of Li^+ in the electrolyte.[12] These are connected through an RC element representing the charge-transfer processes at the $LiFePO_4$/BMABP/electrolyte interface. The Nyquist plot exhibits a short straight line and a semicircle in the intermediate frequency region, depicting the charge transport through the molecular monolayer and charge transfer at the $LiFePO_4$/BMABP/electrolyte interface, respectively, and a tail at low frequencies indicating the diffusion and storage of Li^+ in $LiFePO_4$. The charge-transfer impedance (R_{CT}) can be estimated from the semicircle (R_1C_1). In accordance with the CV shown above, R_{CT} is much smaller at lower Li^+ concentrations in the electrolyte than at higher ones, indicating faster hole injection from the $BMABP^+$ into the $LiFePO_4$ due to the increased driving force for the process. In contrast, the spectrum of the BMABP-derivatized mesoscopic Al_2O_3 electrode shows only capacitive behavior at low frequencies and a Warburg diffusion-like feature at intermediate frequencies, consistent with the absence of Faradaic reactions at the Al_2O_3/BMABP/electrolyte interface.[4c,12]

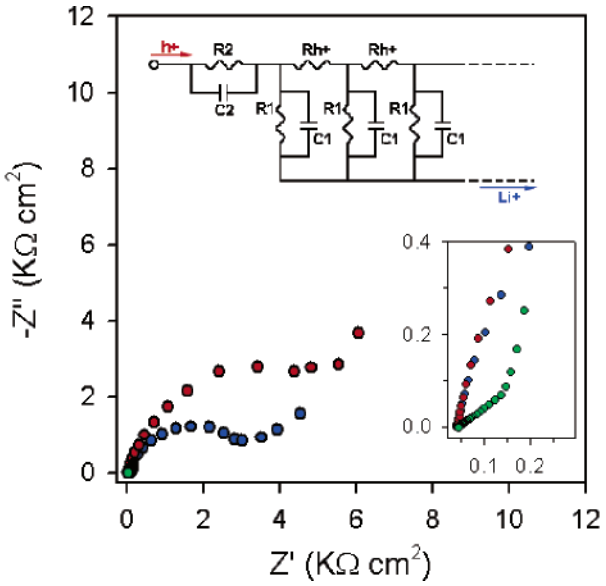

Figure 3. Electrochemical impedance spectra of BMABP-derivatized $LiFePO_4$ (red, blue) and mesoscopic Al_2O_3 (green) electrodes. The insets show the equivalent circuit and an expansion of the spectra in the high-frequency region. The low-frequency tail is not shown in the equivalent circuit. The spectra were obtained at 3.6 V (vs Li^+/Li). The electrolyte was $LiPF_6$ (sat.)/EC+DEC (1:1) except for the blue curve, where 0.5 M $LiPF_6$ was used.

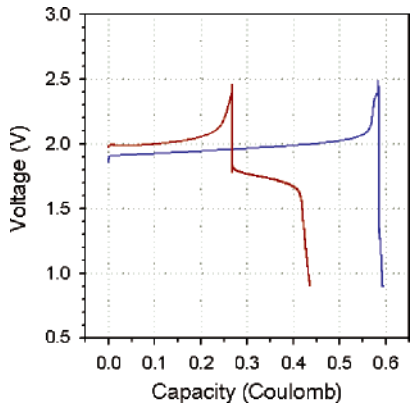

Figure 4. Galvanostatic voltage profiles during the charging/discharging of full cells employing BMABP-derivatized $LiFePO_4$ as positive electrodes. The negative electrodes were $Li_4Ti_5O_{12}$. Red curve: the current density is 0.0063 mA/cm^2 when $LiPF_6$ (sat.)/EC+DEC (1:1) was used as the electrolyte. Blue curve: the current density is 0.063 mA/cm^2 when 0.5 M $LiPF_6$/EC+DEC (1:1) was used as the electrolyte.

To prove our concept that a low conductivity lithium insertion battery material can be charged and discharged using a molecular relay as the sole conductive additive, a full cell consisting of $Li_4Ti_5O_{12}$ and BMABP wired $LiFePO_4$ as negative and positive electrodes, respectively, was assembled and submitted to galvanic cycling. Figure 4 shows voltage profiles obtained in 0.5 M and saturated $LiPF_6$ in EC+DEC (1:1). Voltage plateaus were obtained over a significant charging and discharging range near the expected cell voltage of 1.9 V, indicating that the electrochemical processes at the two electrodes proceed close to the equilibrium potentials, the overvoltage being less than 100 mV at the low current density employed.

These experiments confirm that, during charging, holes flow along the surface by lateral percolation, allowing the particle network to be electrochemically addressed even though $LiFePO_4$ is electronically insulating. Charging is sustained until a

(10) Bard, A. J.; Faulkner, L. R. *Electrochemical Methods: Fundamentals and Applications*, 2nd ed.; John Wiley & Sons: New York, 2000.
(11) Kwon, N. H.; Drezen, T.; Exnar, I.; Teerlinck, I.; Isono, M.; Graetzel, M. *Electrochem. Solid-State Lett.* **2006**, *9*, A277.
(12) Bisquert, J.; Grätzel, M.; Wang, Q.; Fabregat-Santiago, F. *J. Phys. Chem. B* **2006**, *110*, 11284.

significant fraction of $LiFePO_4$ has been converted to $FePO_4$. Conditions to obtain maximum conversion during charging and discharging have yet to be optimized, the main shortcoming of the $LiFePO_4$ material employed here being the large particle size (~400 nm) and low specific surface area (~5 m^2/g). As the lithium extraction from $LiFePO_4$ proceeds, its diffusion time to the surface of the large particles increases[13,14] leading to a local depletion of lithium, which augments the interfacial charge-transfer resistance. To sustain the current, the overvoltage demand increases, requiring conversion of most of the BMABP to $BMABP^+$. As a consequence, the conductivity of the molecular surface layer is decreased, impairing the current flow.

This notion is confirmed by the data obtained with the BMABP-derivatized electrode in a 0.5 M $LiPF_6$/EC+DEC (1:1) electrolyte, where the equilibrium potential for Li^+ extraction is reduced as discussed above, increasing the driving force for hole injection from $BMABP^+$ into $LiFePO_4$. This doubles the lithium extraction capacity as indicated by the blue curve in Figure 4. Our initial experiments show that the reduction of the charge-transfer impedance will be important in reaching high power and energy storage capacities using molecular charge transport layers. Decreasing the $LiFePO_4$ particle size from the current 400 nm to the 50−100 nm size range is expected to offer significant benefits in this regards due to shorter lithium insertion and extraction times as well as reduced surface and interfacial charge-transfer impedance. Further studies are being pursued in this direction, addressing also the question of stability under long-term cycling.

It is worth noting that it is possible to meet even high overvoltage demands during charging and discharging of battery materials by using relay molecules having two reversible couples, the potential of the first couple being slightly lower and the second being slightly higher than the Fermi level of $LiFePO_4$. Thus, holes can be injected from the second and extracted via the first redox process. An example of such a relay molecule is presented in Figure S4.

Conclusions

The results we obtained here with $LiFePO_4$ show that surface bound molecular relays can be used for redox targeting of electro-active materials that are electronic insulators. The phenomena of delivering electronic charge through surface bound molecular "relays" that we observed here for the first time are striking, and their application is expected to extend beyond the field of rechargeable batteries to a wide realm of electronic and bio-electronic devices.

Acknowledgment. We acknowledge financial support of this work by CTI project (contract no. 7136.3 EPRP-IW). We thank Prof. L. Chen and Dr. H. Li at the Institute of Physics, CAS, for kindly supplying the $LiFePO_4$ sample, Dr. R. Humphry-Baker for FTIR measurement, and Mr. P. Comte for mesoscopic Al_2O_3 film preparation and BET measurements.

Supporting Information Available: Adsorption isotherm, FTIR, and other examples of the studied system. This material is available free of charge via the Internet at http://pubs.acs.org.

JA066260J

(13) Prosini, P. P.; Lisi, M.; Zane, D.; Pasquali, M. *Solid State Ionics* **2002**, *148*, 45.
(14) Morgan, D.; Van der Ven, A.; Ceder, G. *Electrochem. Solid-State Lett.* **2004**, *7*, A30.